American Mineralogist, Volume 91, pages 1628–1642, 2006

Transformations of Mg- and Ca-sulfate hydrates in Mars regolith

DAVID T. VANIMAN* AND STEVE J. CHIPERA

Earth and Environmental Sciences Division, Los Alamos National Laboratory, MS D462, Los Alamos, New Mexico 87545, U.S.A.

ABSTRACT

Salt hydrates have an active role in regolith development on Mars. The Mg-sulfate system, with highly variable values of n in the formula $MgSO_4 \cdot nH_2O$, is particularly subject to transformations among several crystalline and amorphous forms. The Ca-sulfate system, $CaSO_4 \cdot nH_2O$, is likely to be associated with the Mg-sulfates in most occurrences, but is less susceptible to transformations in n. Desiccation of $MgSO_4 \cdot nH_2O$ occurs in exposed soils at the martian equator in summer where higher daytime temperatures at low relative humidity prevail against sluggish nighttime rehydration at high relative humidity. Desiccation and rehydration are both accelerated in the finest size fractions, particularly in silt-size aeolian particles subject to global redistribution by dust storms. This redistribution and periodic excursions into long-term episodes of high obliquity work to rehydrate desiccated $MgSO_4 \cdot nH_2O$ to form epsomite, $MgSO_4 \cdot 7H_2O$, at higher latitudes in the first case and more globally in the latter. Kieserite, a monohydrate form of $MgSO_4 \cdot nH_2O$ resistant to desiccation, can survive equatorial summer conditions, but not protracted high relative humidity; preservation of kieserite at the surface may place limits on the equatorial distribution of ice during past episodes of high obliquity. Deeper horizons in equatorial regolith may preserve hydrated phases through repeated obliquity episodes, raising the possibility of an ancient regolith archive of past hydration. At shallower depths in the regolith, in situ determination of the hydration states of the Mg-sulfates, and possibly the Ca-sulfates, may be used to constrain regolith dynamics if rates and modes of transitions in n can be fully characterized.

Keywords: Lunar and planetary studies, crystal growth, phase transition, kinetics

INTRODUCTION

With the Viking landings in 1976, the first chemical analyses of martian soil from near-equatorial and higher latitudes showed that sulfate species are common in the martian near surface (e.g., Toulmin et al. 1977; Clark 1993). The three subsequent landers—Pathfinder in 1997 and the two 2004 Mars Exploration Rovers (MER), Spirit and Opportunity—all found similar occurrences of soil sulfates at widespread locations (Larsen et al. 2000; Rieder et al. 2004). The case for widespread sulfates has been strengthened from orbit with recent visible-near infrared (VIS-NIR) spectral data from the Mars Express OMEGA spectrometer (e.g., Bonello et al. 2005; Langevin et al. 2005). The evidence for Mg-sulfate and Ca-sulfate salt hydrates is now particularly strong, supported by a robust and diverse data set of alpha-proton X-ray Spectroscopy (APXS) data plus thermal emission spectroscopy (THEMIS and TES) data (e.g., Clark et al. 2005; Lane 2005; Squyres et al. 2004). Evidence is also accumulating for the presence of Fe^{3+}-sulfate salt hydrates (Lane et al. 2004), and the hydroxylated Fe^{3+} sulfate mineral jarosite has been identified specifically by Mössbauer data from the MER rover Opportunity (Klingelhöfer et al. 2004), but the available data indicate that Mg- and Ca-sulfates have more widespread distribution among salts on Mars.

Clark and coworkers (Clark 1978; Clark and Van Hart 1981) have considered the implications of salty martian regolith and evaluated salt abundances. In least-squares analyses of Viking and Pathfinder data, they used a postulated salt component based on a mixture of the Mg-sulfate mineral kieserite ($MgSO_4 \cdot H_2O$), with a much smaller amount of halite plus sylvite to account for measured chloride (Larsen et al. 2000). This approach yielded chemical soil models for Pathfinder and Viking 1 with weight proportions of 10.0% $MgSO_4$ (anhydrous basis) in average Pathfinder soil and 13.7% at Viking 1. As in previous work (e.g., Baird et al. 1976), they noted that shallow duricrust at Viking 1 is enriched in this sulfate component relative to uncemented soil. In these and similar studies, the correlation between Mg and S in regolith chemical analyses consistently implicates some form of $MgSO_4 \cdot nH_2O$.

In addition to the Mg-sulfates, there is strong evidence from martian meteorites, rover chemical analyses, and orbital spectroscopy for the presence of Ca-sulfates. Studies of many martian meteorites have found $CaSO_4 \cdot nH_2O$ as a component in fracture fillings that formed on Mars (Bridges et al. 2001; Gooding et al. 1991). Most compelling are the recent APXS data from the MER rover Opportunity indicating an association of Ca-sulfate with Mg-sulfate in the sedimentary outcrops of Meridiani Planum (Clark et al. 2005) and the UV-VIS data from the OMEGA spectrometer on Mars Express. The OMEGA data have revealed widespread gypsum in surface soils at high latitude (Langevin et al. 2005) and gypsum plus hydrated Mg-sulfates and possible Fe-bearing sulfates in layered terrain at Valles Marineris,

* E-mail: vaniman@lanl.gov

Margaritifer Sinus, and Terra Meridiani (Gendrin et al. 2005). These data indicate a significant role for $CaSO_4 \cdot nH_2O$, along with $MgSO_4 \cdot nH_2O$, in both rocks and regolith on Mars.

In an earlier paper, we briefly addressed the issue of desiccation and hydration of Mg-sulfates at the martian surface, with potential formation of a desiccated but still water-bearing amorphous form at lower latitudes (Vaniman et al. 2004a). In this paper, we provide a more detailed analysis of these processes and expand our studies to the Ca-sulfate system, following evidence that Mg- and Ca-sulfates are both constituents of martian sediments and that they may be related genetically (Vaniman et al. 2004b). The goal of the present study is to integrate petrographic, X-ray diffraction, and gravimetric analyses of Mg- and Ca-sulfate formation, desiccation, and hydration processes to form a conceptual model of how these salt hydrates may be distributed in the martian regolith. In addition, we provide a preliminary assessment of how vulnerable the hydration states of these salts may be to transformation during aeolian transport or under ice redistribution to lower latitudes at conditions of higher martian obliquity (greater spin axis tilt).

Prior studies: Sulfate hydrates, hydrous silicates, and near-surface water on Mars

Results from the Mars Odyssey orbital neutron experiment (Feldman et al. 2004a; Basilevsky et al. 2003) suggest the presence of extensive equatorial regions, such as Arabia Terra, with up to ~10 wt% H_2O-equivalent hydrogen abundance, amounts difficult to reconcile with the likely absence of shallow water ice at the equator (e.g., Mellon and Jakosky 1993, 1995). Previously we have considered the potential inventories of near-surface equatorial water that might be held in clays and zeolites (Bish et al. 2003), minerals suggested to be present on the basis of either modeling of soil chemical and water-loss properties (Toulmin et al. 1977) or analysis of spectra from orbit (e.g., Ruff 2004; Poulet et al. 2005).

Bish et al. (2003) concluded that at typical martian P_{H_2O} (~1.5×10^{-6} bars; ~0.1 Pa) and near-equatorial diurnal temperature cycling, Na-smectites retain more water than Ca-smectites, but both are likely to exchange water on a daily basis if in contact with atmosphere. The skin depth for this diurnal cycling is likely to range from a few millimeters to a few centimeters (Möhlmann 2004; Schorghofer and Aharonson 2005); however, the skin depth for seasonal exchange can be on the order of tens of centimeters (Schorghofer and Aharonson 2005). The actual depths to which these cycles penetrate will depend on several factors, including diffusivity, thermal inertia, albedo, and slope orientation (Schorghofer et al. 2002; Schorghofer and Aharonson 2005).

Data for zeolites indicate that clinoptilolite also will exchange water under these conditions, but to a lesser extent, and other zeolites such as chabazite may remain largely hydrated, particularly in the highest-energy H_2O sites (Fialips et al. 2005a). These studies show that if zeolites such as clinoptilolite or chabazite were present in the martian regolith, they would be 90 to 100% hydrated, with H_2O contents of up to ~20 wt%, and smectites could hold about half that amount. For example, the average H_2O content of most equatorial regions, ~4%, can be accounted for by ~40% Ca-smectite or 20% chabazite, without calling on any hydration of duricrust salts recognized in such terrains by the Viking landers. However, large amounts of clay or zeolite (30–70%) would be required in the upper 1 m to account for values as high as 10 wt% H_2O in Arabia Terra, as cited above (Fialips et al. 2005b). In general, the amounts of water observed in the shallow subsurface near the martian equator cannot reasonably be accounted for by hydrated silicate minerals alone (Bish et al. 2003; Fialips et al. 2005b). As a consequence, it is likely that hygroscopic salts have a significant role in accounting for hydrated regolith at low martian latitudes.

Recent OMEGA data emphasize the presence of clays in older, Noachian terranes on Mars (Poulet et al. 2005), but sulfates appear to be the dominant mineral hydrates in younger systems (Gendrin et al. 2005; Langevin et al. 2005). The origins of these sulfates may be varied, stemming in part from sedimentary deposits (Solomon et al. 2005) and forming throughout later episodes from other forms of water-rock interaction, such as weathering by volcanic "acid fog" (Banin et al. 1997; Tosca et al. 2004). Active mid-latitude "slope streaks" that may be formed by brine discharges (e.g., Knauth and Burt 2002; Schorghofer et al. 2002) suggest that brine-regolith interactions could be taking place on Mars today. Regardless of primary origin, whether ancient or modern, sulfate salts are distributed widely across the surface of Mars, possibly by a combination of processes including impact distribution and eolian transport. We summarize below some of the fundamental data on the two salt systems that are the focus of this study, the simple Mg- and Ca-sulfates, as found on Earth and inferred on Mars.

Magnesium sulfates

The Mg-sulfate mineral system (Table 1a) contains several hydrated crystalline and amorphous phases of $MgSO_4 \cdot nH_2O$, including crystalline 7-, 6-, 5-, 4-, 2-, and 1-hydrates and amorphous phases that hydrate and dehydrate under conditions influenced by P_{H_2O} and temperature. The only common members of the $MgSO_4 \cdot nH_2O$ series on Earth are epsomite ($MgSO_4 \cdot 7H_2O$, orthorhombic, $P2_12_12_1$, 51 wt% H_2O), hexahydrite ($MgSO_4 \cdot 6H_2O$, monoclinic, $C2/c$, 47 wt% H_2O), and kieserite ($MgSO_4 \cdot H_2O$, monoclinic, $C2/c$, 13 wt% H_2O; structures cited here are from Hawthorne et al. 2000). Occurrences are varied, including evaporite deposits (the principal occurrence of kieserite), mine or cave efflorescence, fumaroles, and acid weathering of monuments and structures. Some environments of formation are extremely tenuous. For example, kieserite, along with thenardite, blödite, and gypsum, has even been found to precipitate on grasses from acid fogs with high sulfate content produced by powerplants (Singer et al. 1999). Rarer minerals of the $MgSO_4 \cdot nH_2O$ series are pentahydrite ($MgSO_4 \cdot 5H_2O$, triclinic, $P\bar{1}$, 43 wt% H_2O), starkeyite ($MgSO_4 \cdot 4H_2O$, monoclinic, $P2_1/n$, 37 wt% H_2O), and sanderite ($MgSO_4 \cdot 2H_2O$, structure unknown, 23 wt% H_2O). All minerals of the $MgSO_4 \cdot nH_2O$ series consist of SO_4 tetrahedra and $Mg(O,H_2O)_6$ octahedra; some include extra-polyhedral water. Epsomite transforms readily to hexahydrite by loss of the one water molecule per 7-water formula unit that is not octahedrally coordinated with Mg (Hawthorne et al. 2000); this transition occurs at ~50–55% relative humidity (RH) at 295 K and at lower temperature as RH diminishes (Chou and Seal 2003). The structure of kieserite is unique in the $MgSO_4 \cdot nH_2O$ system, consisting of a three-dimen-

sional infinite framework in which tetrahedral-octahedral chains of SO_4 and $Mg(O_5H_2O)$ are cross-linked by shared corners between octaheda and tetrahedra of adjacent chains (Hawthorne et al. 2000; Grodzicki and Piszczek 1998). This structure is much more resistant to dehydration than those of the other $MgSO_4{\cdot}nH_2O$ minerals (Chipera et al. in prep.), and survives to temperatures >570 K in thermal analysis experiments.

Available data on the Mg-sulfate hydrates indicate that the hydration state near or at the martian surface is likely to vary with latitude (Zolotov 1989; Feldman et al. 2004b), with epsomite generally stable at higher latitudes and less hydrated forms distributed toward the equator. Epsomite stability at higher latitudes will be favored where water ice is stable; this stability boundary will vary between the latitudes of ~50 to 70° as seasons shift (Schorghofer and Aharonson 2005), providing an extensive mid-latitude swath where surface conditions favorable to epsomite may vary over annual time cycles equivalent to two Earth years. Moreover, for longer periods, of approximately ~10^4–10^5 Earth years, changes in obliquity at Mars have favored redistribution of much of the polar water ice toward the equator (Mellon and Jakosky 1995; Head et al. 2003). Full hydration of low-*n* species to epsomite will depend on whether these cycles provide enough time to reach that state at the low temperatures and low values of P_{H_2O} involved, where hydration reactions will be sluggish. Some preliminary conclusions are reached in this paper; more complete data on desiccation and hydration rates at low temperature are being collected and will be reported in a subsequent paper. Such studies are important because the regolith distributions of different hydration states of $MgSO_4{\cdot}nH_2O$ are likely to be dynamic across much of Mars, with consequences for understanding the present retention of water in regolith and the origin and subsequent history of salt hydrates in primary sediments and derivative soils (Vaniman et al. 2004a).

Calcium sulfates

The common calcium sulfate minerals (Table 1b) are gypsum ($CaSO_4{\cdot}2H_2O$, monoclinic, $I2/c$, 21 wt% H_2O), bassanite ($CaSO_4{\cdot}0.5H_2O$, trigonal, $P3_12$, 6 wt% H_2O), and anhydrite ($CaSO_4$, orthorhombic, *Amma*, anhydrous). The structures cited here are from Hawthorne et al. (2000) or references therein, but there are significant differences in the literature that may have petrogenetic implications (see, for example, the discussion of various Ca-sulfate hemihydrates by Follner et al. 2002, suggesting that α and β forms can reflect acidic precipitation vs. hot desiccation, respectively). Anhydrite and bassanite occur most commonly in situations where thermal processing is likely to have dewatered precursor gypsum, in late-stage evaporite assemblages where the residual activity of water in the brine is very low, or in acid alteration environments. Gypsum has a very widespread occurrence in evaporite deposits and other sediments, as a vadose-zone fracture mineral, as cave and mineshaft speleothems, in fumaroles, and in ore deposits. Of particular importance for regolith studies, gypsum also occurs as distributed crystals in dry soils, including those of the Dry Valleys in Antarctica often cited as Mars analogs (e.g., Wentworth et al. 2005: Ca-sulfate likely to be gypsum). In environments where sources of Ca and sulfate are abundant, gypsum in soils can be extensive enough to form cemented soil horizons classified as gypcrete (e.g., Aref 2003). Also of importance is the common formation of gypsum as an acid alteration product of limestone (Table 1b), an association that may in part explain the widespread occurrence of gypsum and other sulfates rather than carbonate minerals in martian sediments and regolith.

Much is known about the transitions between $CaSO_4{\cdot}nH_2O$ forms because of their very long history of use and worldwide importance as plasters and cements. It is therefore somewhat surprising and, for our purposes, sobering to realize that questions remain about how many values *n* might take as discrete phases (e.g., Adam 2003). This problem illustrates the difficulty in pinning down the environmental controls over *n* in deposits of salt hydrates. Present data for Mars point to the presence of hydrated $CaSO_4{\cdot}nH_2O$, but do not distinguish between gypsum and bassanite (Gendrin et al. 2005).

METHODS

The methods used in this study include synthesis of pure Mg-sulfate minerals (for Ca-sulfate studies, a natural gypsum from Bingham, New Mexico was used). Analytical methods used were powder X-ray diffraction (XRD) at room conditions or in an environmental cell at various controlled temperatures with controlled relative humidity (RH), thermogravimetric analysis at controlled heating rates, and scheduled weighing of hydrating or dehydrating samples in isothermal experiments. Isothermal dehydration was either monitored by real-time XRD in the environmental cell or observed over longer time spans by periodic analysis of samples held in a vacuum chamber. Isothermal rehydration was monitored with samples held at 100% RH over water or water ice at various temperatures. The

TABLE 1A. Minerals, water, and associations in the Mg-sulfate system

Mg-Sulfate Hydrates: Structural Types* and Mineral Names	Wt% H_2O	Representative Associations
Isolated SO_4 tetrahedra		
Epsomite ($MgSO_4{\cdot}7H_2O$)	51	"acid rain" alteration, caves, mines, saline lakes
Hexahydrite ($MgSO_4{\cdot}6H_2O$)	47	"acid rain" alteration, thermal springs, fumaroles, mines, saline lakes
Chains of SO_4 tetrahedra		
Pentahydrite ($MgSO_4{\cdot}5H_2O$)	43	mines, geysers
Clusters of SO_4 tetrahedra		
Starkeyite ($MgSO_4{\cdot}4H_2O$)	37	mines (oxidized pyrite and marcasite)
Structure (?)		
Sanderite ($MgSO_4{\cdot}2H_2O$)	23	Mines
SO_4 framework structures		
Kieserite ($MgSO_4{\cdot}H_2O$)	13	salt and potash mines

Note: Hydration states of $n = 12, 3, 1.25$, and 0 can be synthesized but have not been recognized as minerals.
* Structural classification based on Hawthorne et al. (2000).

TABLE 1B. Minerals, water, and associations in the Ca-sulfate system

Ca-Sulfate Hydrates: Structural Types* and Mineral Names	Wt% H_2O	Representative Associations
Sheets composed of edge-sharing chains of alternating SO_4 tetrahedra and CaO_8 dodecahedra		
Gypsum ($CaSO_4{\cdot}2H_2O$)	21	the most common sulfate mineral: evaporites, caves, mines, authigenic in soils (gypcrete), gypsum sands (aeolian) and gyparenite sandstones, secondary gypsite efflorescence, "acid rain" alteration, acid-sulfate alteration of limestone deposits
Anhydrite ($CaSO_4$)	0	evaporites, acid-sulfate alteration of limestone, fumaroles
Framework composed of cross-linked chains of alternating SO_4 tetrahedra and CaO_9 polyhedra		
Bassanite ($CaSO_4{\cdot}0.5H_2O$)	6	evaporites, fumaroles

* Structural classification based on Hawthorne et al. (2000).

methods used are summarized in Table 2; details are provided below. All experiments and measurements were carried out using facilities at LANL.

Epsomite, hexahydrite, and kieserite synthesis

The epsomite, hexahydrite, amorphous $MgSO_4 \cdot nH_2O$, and brines used in this study were synthesized from Alfa Aesar Puratronic reagent marketed as $MgSO_4 \cdot xH_2O$. At the temperature and RH conditions in our laboratory, this product is mostly in the form of hexahydrite, with pentahydrite forming at dry winter conditions (phase confirmation by XRD). This ultrapure (99.997%) reagent was used to avoid complications from the ~0.03% Ca that is a common constituent in standard reagents. This impurity can be a concern where formation of $CaSO_4 \cdot nH_2O$ phases must be avoided or controlled. Epsomite crystals were grown from solution in deionized water. These crystals and powders prepared from them were aged before use at 297–298 K and at a relative humidity (~75% RH; ~2300 Pa P_{H_2O} at this temperature) controlled over saturated solutions of NaCl. These conditions maintain the sample within the stability field of epsomite and prevent dehydration to hexahydrite or pentahydrite, which would occur at humidity conditions prevalent in our laboratory. Some epsomite samples were converted to hexahydrite by exposure for a few days at summer room conditions of 298 K and 30–40% RH. Kieserite was formed from Fisher Scientific magnesium sulfate certified anhydrous reagent (containing 0.03% Ca) by placing aliquots in a sealed Teflon vessel over a saturated-salt solution of $SrCl_2$ at 348 K (controlling RH at ~63%) for periods of greater than 3 weeks. All syntheses were confirmed by XRD.

X-ray diffraction

Powder X-ray diffraction (XRD) data were obtained on an automated Siemens D500 diffractometer using Cu$K\alpha$ radiation, incident- and diffracted-beam Soller slits, and a Kevex Si(Li) solid-state detector, measuring from 2 to 70 °2θ. Data were collected in two different sample management configurations. Single-pass analyses of relatively stable single- or multi-phase samples were collected using sample holders open to atmosphere, with scan times of ~4 h. Long-duration analyses, of up to two weeks on a single sample, were performed in an environmental cell that controls humidity by flowing a mixture of dry nitrogen and 100% RH water vapor monitored by a Vaisala humidity meter connected to gas-mixing controls. Temperature inside the environmental cell was 300 K at ambient conditions, but samples also can be heated in the environmental cell. A detailed description of this system is provided in Chipera et al. (1997).

Samples of clays, zeolites, and palagonite were made into slurries with saturated room-temperature solutions of Alfa Aesar ultrapure $MgSO_4 \cdot xH_2O$. These mixtures were degassed in the vacuum chamber at pressures of ~2 torr for ~20 min. The products were then examined by XRD to determine the sulfate phases present after interaction with these representative "soil" silicate phases. Clays used included smectite from Succor Creek, Oregon, and two Clay Minerals Society source clays, ferruginous smectite SWa-1 and nontronite NG-1. Zeolites used included chabazite from Christmas, Arizona, and clinoptilolites from the Fish Creek Mountains, Nevada, and from Castle Creek, Idaho. The palagonite used was martian soil simulant JSC-1 from Pu'u Nene cinder cone on the Island of Hawaii (Allen et al. 1998). Compositions of these samples are listed in Table 3.

Thermogravimetric analysis

Thermogravimetic analyses of sample water content and of water loss temperatures and rates were collected on a DuPont 951 Thermogravimetric Analyzer. Samples prone to rapid loss of water (e.g., epsomite) or gain of water (desiccated amorphous forms) at room conditions were removed directly from their controlled atmospheres and loaded on the balance pan within ~2 min. For most of the data reported here, standard heating rates of 10 °C/min and dry N_2 flush were used. Some epsomite samples were analyzed at the same conditions but with dry CO_2 flush; with CO_2 flush weight loss curves were very slightly higher (shifted by ~4 °C), but were otherwise unchanged.

Vacuum chamber desiccation

A VWR 1410D vacuum oven at room temperature (297 to 298 K) and roughing-pump vacuum conditions of ~0.5–1.0 torr was used for examination of long-term desiccation effects at temperature and P_{H_2O} conditions approaching those of the martian equatorial surface on a hot summer day. Samples of synthetic epsomite, hexahydrite, and kieserite, and natural selenite gypsum (from Bingham, New Mexico) were maintained at these conditions for periods of one week to 11 months. For these room-temperature experiments, sample holders were made of thin-wall polystyrene cups with perforated lids. For experiments at higher temperature, crimped thin-wall aluminum containers with perforated tops were used. Sample masses used in all experiments were ~200 mg. Samples were removed and weighed periodically for periods of ~5 min; weight drift during weighing was monitored and is within 0.5% of the sample mass. For most experiments, temperature within the chamber varied from 297 to 298 K, and the effective P_{H_2O} from evacuation of bled-in room humidity ranged from 0.2 to 1.3 Pa (av. 0.7 Pa; equivalent RH of ~0.02%). Some preliminary desiccation rates for epsomite at higher temperature were obtained at 323 K, with the same estimated P_{H_2O} and an equivalent RH of ~0.005%.

Rehydration at 100% RH

Samples of amorphous forms of $MgSO_4 \cdot nH_2O$, kieserite, and desiccated gypsum (effectively, dewatered bassanite) were rehydrated at 100% RH over water or water ice. Rehydration was performed at room temperature (297 K), in a lab refrigerator (277 K), and in three lab freezers (271, 243, and 193 K). Experiments at temperatures below 243 K are ongoing and are not reported here. As with the room-temperature desiccation experiments, sample holders were made of thin-wall polystyrene cups with perforated lids; sample masses typically began at ~100–150 mg, rising to ~200 mg in the rehydrated forms. Samples were removed and weighed periodically for periods of ~2 min; weight drift during weighing was monitored and is within 0.5% of the sample mass.

TABLE 2. Summary of methods used

1 Syntheses		2 X-ray diffraction	3 Gravimetric analysis	4 Vacuum chamber desiccation	5 Hydration at 100% RH
Pure phases	**Epsomite** (purified at 298 K over NaCl saturated solution) **Hexahydrite** (exposure of epsomite to summer room conditions of 298 K and 30–40% RH) **Kieserite** (purified at 348 K over $SrCl_2$ saturated solution)	**<4 h**: powder XRD at room conditions **>4 h**: powder XRD in environmental cell with RH control (input range 0–100% RH at room temperature) and temperature control (300 to 350 K)	**Standard thermogravimetric** analysis (TGA) at 10 °C/min with dry N_2 or CO_2 flush **Scheduled periodic** weighing of isothermal hydrating or dehydrating samples with an analytical balance	Desiccation at 0.5–1.0 torr and ~0.7 Pa P_{H_2O} at either 297-298 K (0.02% RH) or 323 K (0.005% RH)	Hydration over water or water ice at 297, 277, 271, or 243 K
Mineral mixtures	**Brine slurries** (saturated $MgSO_4$ solutions mixed with zeolites, clays, or palagonite) evacuated at ~2 torr in open containers **Brine smears** (saturated $MgSO_4$ solutions mixed with zeolites, clays, or palagonite) evaporated on thin sections, beneath cover slips, at room conditions				

TABLE 3. Compositions of clays, zeolites, and palagonite used in brine evaporation studies

	Ferruginous Smectite SWa-1: Grant County, Washington	Nontronite NG-1: Hohen Hagen, Germany	Smectite: Succor Creek, Oregon	Clinoptilolite: Castle Creek, Idaho	Clinoptilolite: Fish Creek mountains, Nevada	Chabazite: Christmas, Arizona	Palagonite JSC-1: Pu'u Nene, Hawaii
SiO_2	43.8	45.8	53.0	62.8	67.2	53.1	34.5
TiO_2	0.54	0.05	0.56	0.32	0.11	0.32	3.0
Al_2O_3	7.95	5.93	16.6	12.6	12.0	14.7	18.5
Fe_2O_3	25.3	32.2	11.1	2.35	1.29	1.88	12.4
MgO	1.75	1.02	2.02	1.57	1.13	2.7	2.7
CaO	2.05	1.95	1.09	1.38	2.82	3.40	4.9
Na_2O	0.00	0.03	1.28	2.86	0.81	3.5	1.9
K_2O	0.03	0.13	0.13	1.52	3.06	1.50	0.5
LOI*	19.4	13.4	8.93(14.2)	14.4	9.1(11.5)	18.4	21.8

Notes: Compositions for SWa-1 and NG-1 via Clay Minerals Society; Christmas, Arizona chabazite data from Sheppard and Gude (1982); JSC-1 palagonite analysis from Allen et al. (1998). Analyses by X-ray fluorescence, induction coupled plasma and/or atomic absorption.
* LOI is loss on ignition at 900 or 1000 °C, a reasonable approximation of total water content in these samples. Note that water content in clays and zeolites varies rapidly with changes in room temperature and RH; values in parentheses indicate likely water content when LOI was collected under different room conditions than when the sample was weighed for chemical analysis.

Petrographic analysis (single crystals and brine-detritus mixtures)

Single crystals of epsomite and of hexahydrite or amorphous pseudomorphs after epsomite were examined and photographed with a binocular microscope and with a standard petrographic microscope equipped with both transmitted and reflected light. Portions of the hexahydrite pseudomorphs after epsomite were also fragmented and analyzed as grains in oil. For brine interaction experiments, clays, zeolites, and palagonite were made into smears with saturated solutions of Alfa Aesar ultrapure $MgSO_4 \cdot xH_2O$. These smears were made on thin-section slides beneath cover slips and allowed to desiccate from the edges inward at room conditions. The petrographic microscope was used to identify the sulfate phases formed in sequences of brine crystallization and to examine textures developed in the smear samples.

RESULTS

Physical observations of epsomite crystals in dehydration-rehydration cycling

Single crystals of epsomite were dehydrated to form hexahydrite at room conditions (298 K, 30–40% RH or 950–1270 Pa P_{H_2O}), then desiccated further in a vacuum chamber at 297–298 K and ~0.7 Pa P_{H_2O} to form amorphous products. The amorphous forms were then rehydrated at a P_{H_2O} (518 Pa) controlled by water ice at 271 K. Figure 1 shows a representative epsomite starting crystal (Fig. 1a), followed by pseudomorphs of hexahydrite formed at room conditions after 800 h (Fig. 1b), amorphous after 170 h in vacuum (Fig. 1c), and rehydrated second-generation epsomite after 360 h at 271 K with P_{H_2O} controlled by water ice (Fig. 1d). The dehydration times cited here are longer than required for hexahydrite or amorphous phase formation and are not intended to imply rate, whereas the rehydration time of 360 h is the monitored time required to re-form epsomite completely in this sample (i.e., transition of Fig. 1c to 1d). The pseudomorph of hexahydrite after epsomite (Fig. 1b) loses the transparency of epsomite. Loss of 1/7 of epsomite water from the interior of the crystal to produce hexahydrite occurs along tight fractures that are locally cuspate (Fig. 1b1), with arc radii similar to those of spherulitic clusters of elongate length-fast hexahydrite grains within the pseudomorph (Fig. 1b2). The cuspate fracture pattern shows that fractures for dehydration follow the margins of larger spherulitic or fan-shaped clusters rather than the very small (<10) μm hexahydrite grains within the clusters.

Monitoring of the desiccation process by XRD in the environmental cell shows that loss of hexahydrite structure to produce an X-ray amorphous form occurs at this very low RH without transitional formation of intermediate crystalline hydrates (e.g., Fig. 1 in Vaniman et al. 2004a). Dehydration from epsomite to hexahydrite and then to an amorphous but partially hydrated phase under these conditions involves a weight loss of 43%, but the amorphous pseudomorph after epsomite (Fig. 1c) does not change in volume. In large single crystals, the amorphous

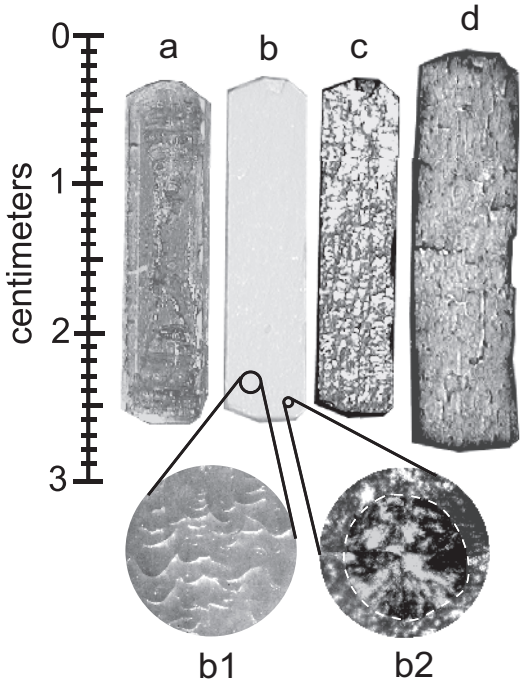

FIGURE 1. Transitions of a single epsomite crystal (**a**) to hexahydrite (**b**) at room conditions (298 K, 30–40% RH or 950–1270 Pa P_{H_2O}), to amorphous (**c**) after 170 h at 297 K and ~0.7 Pa P_{H_2O}, and back to epsomite (**d**) after 360 h at 271 K and 518 Pa P_{H_2O} (100% RH over water ice). Note that the pseudomorphs after epsomite retain original dimensions through form **c**, as fractures allow water loss but maintain gross morphology; in **d,** regrowth of epsomite in a mosaic of offset orientations remains intact but results in ~70% volume expansion. Insets show the intersection with the hexahydrite surface of cuspate fractures that provide pathways for loss of 1/7 of the epsomite water (reflected light photo **b1**; diameter of circle 1.1 mm) and spherulitic growth of small hexahydrite grains (transmitted cross-polarized light photo **b2**; diameter of dashed circle outlining the spherulite is 200 μm).

pseudomorph shows development of a network of open shrinkage cracks with spacing of <1 mm (gray fractures seen in Fig. 1c), larger in aperture than the cuspate cracks in the hexahydrite pseudomorph (Fig. 1b1). Despite more extensive fracture development, the amorphous pseudomorph maintains the dimensions and habit of the original orthorhombic epsomite crystal. When this amorphous pseudomorph after epsomite is rehydrated slowly at 100% RH and 271 K, forming second-generation epsomite, the habit is generally retained but the size increases by 16–22% (avg. 19%) along the A, B, and C axes. If kept at 271 K and 518 Pa P_{H_2O} this form can persist for at least 8 months, even though it is slightly above the liquidus (Chou and Seal 2003). If rehydrated at higher temperature and P_{H_2O}, over liquid water rather than ice, the sample will deliquesce, drawing in enough water from the atmosphere to form a solution within a few days.

Brine-detritus interactions

Figure 2 shows XRD analyses of representative products of saturated $MgSO_4$ brines mixed with three different "detrital" materials: Castle Creek clinoptilolite, palagonite JSC-1, and ferruginous smectite SWa-1 (Table 3). These mixtures of brine with silicate phases were forced to desiccate and crystallize within 20 min at ~2 torr total pressure and 297 K. The rapid slurry evaporation experiments were designed to approximate release of brine into shallow regolith near the martian surface as may be occurring where slope streaks have been observed (Knauth and Burt 2002). The pure starting solution of $MgSO_4$ brine was used not to represent a realistic model of martian brine, but to understand a simpler system. Similarly, simple monomineralic hydrous silicates were used to understand brine reactions with individual minerals, although a palagonite also was used to examine reactions with more complex materials. In all cases, hexahydrite forms from the brine on low-pressure crystallization, but gypsum also formed (the hexahydrite and gypsum would lose much of their water content and transform to amorphous $MgSO_4 \cdot nH_2O$ and bassanite, respectively, if held at vacuum as described below).

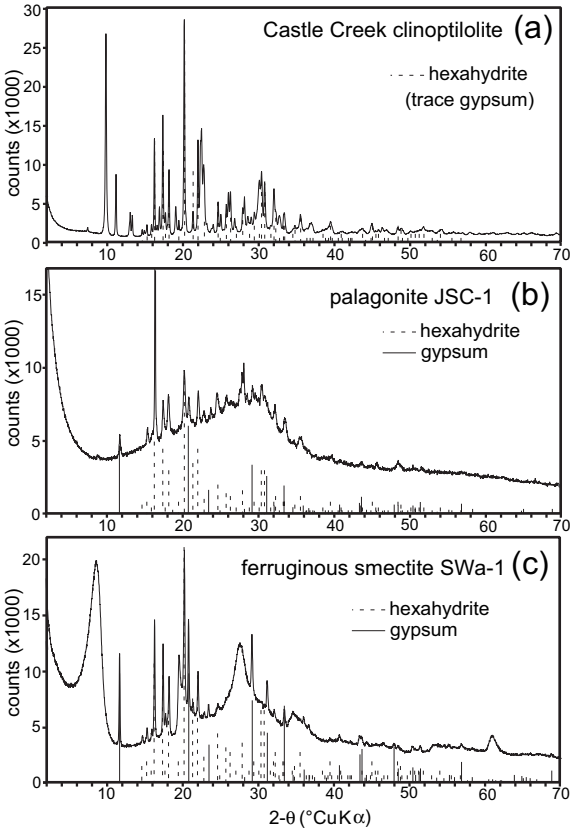

FIGURE 2. X-ray diffraction (XRD) patterns of $MgSO_4$ brine-"detritus" slurries solidified by rapid evaporation at ~2 torr. Slurries were formed by mixing pure $MgSO_4$-saturated brines with (**a**) Castle Creek clinoptilolite, (**b**) palagonite JSC-1, and (**c**) clay SWa-1. The characteristic diffraction peak locations and relative intensities for the salts formed are indicated by dashed lines (hexahydrite) and solid lines (gypsum).

As there is no Ca in the brine used, Ca must be extracted from the "detrital" phases in order for gypsum to form. The highest ratio of gypsum to hexahydrite occurred in the clay samples, followed by the palagonite, with only trace amounts of gypsum formed from the zeolitic samples. This sequence appears to be unaffected by relative Ca contents of the clays vs. zeolites, which are generally similar (Table 3). The poor production of gypsum in the zeolite slurries is due at least in part to greater selectivity for Ca than Mg in both clinoptilolite and chabazite (Ames 1961), but the rapid desiccation in these experiments also reduced the time available for exchanging Mg for Ca in the zeolite framework, a factor of less importance in the more-accessible clay interlayers. It is worth noting that when observed in the experiments under cover slips, the clay smears develop fracture channels (Fig. 3a) as the clay mass contracts through loss of interlayer water, but such contraction was not observed in the smears made with zeolites. Zeolites have a stronger tendency to retain the waters of hydration associated with their exchangeable cations and, more importantly, they do not collapse structurally as do clays when water is lost.

Figure 3 provides views of brine smears allowed to desiccate at room conditions under cover slips. Desiccation can be observed progressing inward from the edge of the cover slip where a smear is exposed to atmosphere; as sulfate minerals precipitate from the evolving solution, they can be identified readily by optical petrography. In all samples, including smears formed with clays, zeolites, and palagonite, gypsum precipitates either before or along with epsomite. Figures 3a to 3c illustrate the progression of crystallization in a smear formed of $MgSO_4$ brine and the Clay Minerals Society source clay SWa-1 (Table 3). In Figure 3a, the segregation of an initially homogeneous smear can be seen to result in denser clay bodies and brine-filled channels or fractures; the brine channels propagate inward from the margins of the cover slip. Trails of clay particles remain along the axis of each channel as the fractures grow. Although epsomite forms where the heads of the brine fractures are exposed to atmosphere, no salts have yet started to form within the channels. At room temperature, the channeled interior remains without salt crystals for several days, with the brine likely kept near saturation by addition of interlayer water extracted from the clays as the clay mass contracts. Figure 3b shows the first salt formed; surprisingly, this is gypsum rather than epsomite, even

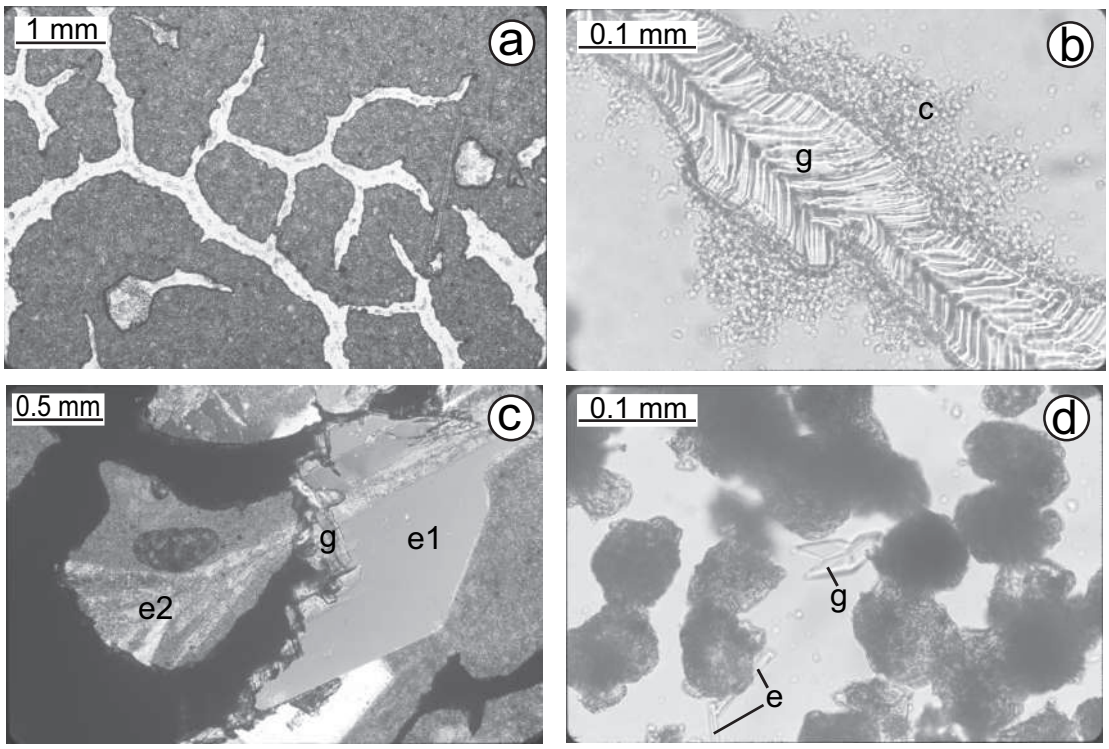

FIGURE 3. Products of $MgSO_4$ brine smear crystallization with clay SWa-1 (**a**–**c**) and palagonite JSC-1 (**d**). With the clay host, brine fractures (**a**) develop first, before salts crystallize. In **b**, gypsum "g" forms early from clay interlayer Ca exchanged with Mg in solution; the gypsum crystals displace particles of clay "c" that were initially left along the axes of fracture channels. In **c**, epsomite has formed after gypsum "g" in displacive "e1" and ultimately cementing "e2" forms. In **d**, Ca extracted from palagonite solids allows early formation of swallowtail-habit gypsum "g" as well as epsomite "e."

though the initial brine solution contained no Ca. It is evident that sufficient Ca has been extracted from the clay interlayers, in exchange for Mg, to form gypsum. These initial gypsum crystals nucleate along the fracture axes and displace clay particles that were distributed along the axes. As water is lost to evaporation at the edges of the system, epsomite eventually forms in the interior. Early interior epsomite (e1 in Fig. 3c) first displaces clay and gypsum but eventually the epsomite penetrates and cements the clay matrix (e2 in Fig. 3c). Figure 3d shows the same salts, gypsum and epsomite, precipitated from a smear formed with Mg-sulfate brine and palagonite JSC-1. Here, the matrix clumps rather than fractures and epsomite forms very soon after gypsum, although again the brine must obtain Ca from the solids, in this case most likely by leaching of glass or other amorphous phases, as no crystalline clays are present in JSC-1 (Fig. 2b; Allen et al. 1998). The salt crystals formed are euhedral, with early-formed gypsum in characteristic "swallowtail" habit.

Desiccation and formation of incompletely dewatered phases

Stability calculations (Zolotov 1989; Feldman et al. 2004b) suggest that epsomite can be stable at the surface at higher latitudes on Mars, where water ice is present or where water vapor in the cold atmosphere is near its frost point (~100% RH). At lower latitudes, however, this is not the case, as very low RH at higher daytime temperatures favors desiccation. To understand better relative water retention in various sulfate hydrates, we have used thermogravimetric analysis (heating at 10 °C/min over ~1 h), XRD analysis of structural transitions at low P_{H_2O} in the environmental cell (day to week timescales), and long-term exposure to vacuum (week to year timescales).

Thermogravimetric analysis. Figure 4 shows the results of standard thermogravimetric analysis of epsomite samples having different grain sizes. Also shown are thermogravimetric analysis curves of a fine powder (<45 μm) of kieserite, a natural gypsum sample (from Bingham, New Mexico), and an amorphous form of $MgSO_4 \cdot nH_2O$ (with $n = 1.25$) prepared by long-term desiccation of epsomite and hexahydrite in the vacuum chamber (gypsum and the amorphous sample are discussed in more detail below). All data were collected at 10 °C/min under flow of dry nitrogen at 60 cc/min.

The epsomite samples have a two-stage water loss, the first corresponding with initial extraction of water of hydration representing the one out of seven structural waters in epsomite that is not octahedrally coordinated with Mg. This is the loosely bound water that is gained or lost readily with shifts in humidity (Chou and Seal 2003), which leads to relatively rapid and reversible transitions between epsomite and hexahydrite. At this heating rate, the finer size fraction has an inflection in the loss curve that comes closest to the composition representing molecular water loss of 1/7 ($n = 6$). The majority of the remaining water loss occurs along deeper curves with 1st derivative minima at 91

to 100 °C (364 to 373 K), depending on particle size. No other discrete deflections in the water loss curves are seen until ~300 °C (573 K), where a small proportion of closely held structural water is released. This release at higher temperature is seen in all epsomite size fractions. We also have observed this release in every form of $MgSO_4{\cdot}nH_2O$ that we have analyzed (Chipera et al. in prep), crystalline or amorphous, except kieserite, which does not begin to lose water below 300 °C (573 K).

Environmental cell analyses. Figure 5 is a plot of 72 sequential XRD analyses in the environmental cell collected with a sample at 336 K and at 6% RH (converted from input RH at ambient temperature to the 336 K sample temperature). Data were collected in a series of XRD scans, from 2 to70 °2θ in 0.02° steps, counting for 4 s/step (each run takes ~4 h), over 12 days. For clarity, Figure 5 shows the data only from 5 to 40 °2θ. The environmental cell data allow direct observation of the rate and nature of phase transitions at selected and controlled P_{H_2O} conditions. The first pattern is that of the starting hexahydrite before taking it to temperature. The second pattern in the sequence shows that the sample is reacting to form an amorphous phase, with some residual hexahydrite, as it is being heated to 336 K. The third pattern in the sequence shows that the sample has gone completely amorphous by the time the XRD pattern was collected (after 8 h). Continued scans show sluggish formation of sanderite (n = 2); with time, the amorphous phase converts completely to sanderite (with a small amount of an unknown Mg-sulfate phase; peaks labeled "u").

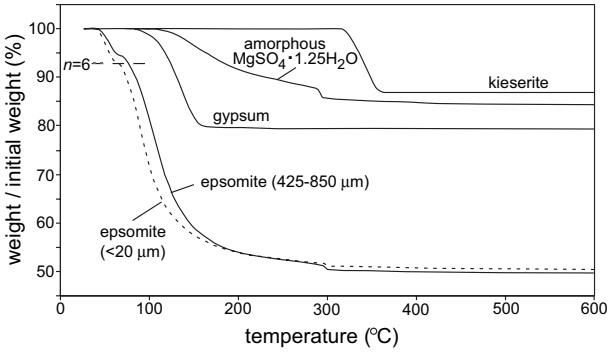

FIGURE 4. Thermogravimetric analyses of representative Mg-sulfate and Ca-sulfate salt hydrates: kieserite ($MgSO_4{\cdot}H_2O$), amorphous $MgSO_4{\cdot}nH_2O$ with n = 1.25, gypsum ($CaSO_4{\cdot}2H_2O$) and two size fractions of epsomite ($MgSO_4{\cdot}7H_2O$). All weight loss curves are for 10 °C/min heating rate with 60 cc/min dry N_2 flush. Dashed horizontal line marks the point of 1/7 water loss in epsomite (point where n = 6) where the most loosely bound water is evolved.

Figure 5 represents many such experiments with various crystalline forms of $MgSO_4{\cdot}nH_2O$ at room temperature or higher, where loss of crystalline structure is simple and monotonic, whereas recrystallization either passes through an amorphous intermediate or introduces several crystalline phases that eventually recrystallize and converge on the stable phase. Depending on distance in T, P_{H_2O} from the reaction boundaries to other hydration forms, convergence can occur in less than a day or may take several months. Companion studies (Chipera et al. 2005; Chipera and Vaniman 2006) summarize the vapor-solid stability regions for phases with n = 6, 4, 2, 1, and 0, using data from both the environmental cell (for transitions that occur within a week) and controlled-humidity salt solutions (for reactions of longer duration). Phases such as amorphous $MgSO_4{\cdot}nH_2O$ are probably metastable products induced by rapid dehydration, as the kinetics of recrystallization are too slow to form a more-stable crystalline phase. Note that the example in Figure 5 is at 336 K; recrystallization rates at low RH are even slower at the lower temperatures more relevant to the martian surface. Like other $MgSO_4$ hydrates, the amorphous phase may require a certain activation energy before it transforms to another phase.

Desiccation in the vacuum chamber. Single crystals, powders, and sieved size fractions of epsomite were desiccated in the vacuum chamber at 0.5 to 1.0 torr and at temperatures of 297 and 323 K (e.g., Fig. 6a). The primary goal of these experiments was to determine desiccation effects at low P_{H_2O} over long timespans, up to 11 months. At both temperatures, there are notable particle size effects in an initial dehydration phase, persisting for ~10 h at 297 K and 2 h at 323 K. Beyond that stage, all size fractions follow the same weight loss path at a given temperature, reaching a point of incomplete desiccation but relatively stable water content. The time required to reach this relatively invariant water content in the amorphous phase is about 4000 h at 297 K (n = 1.2) and 500 h at 323 K (n = 0.9). The sample at 297 K was held at

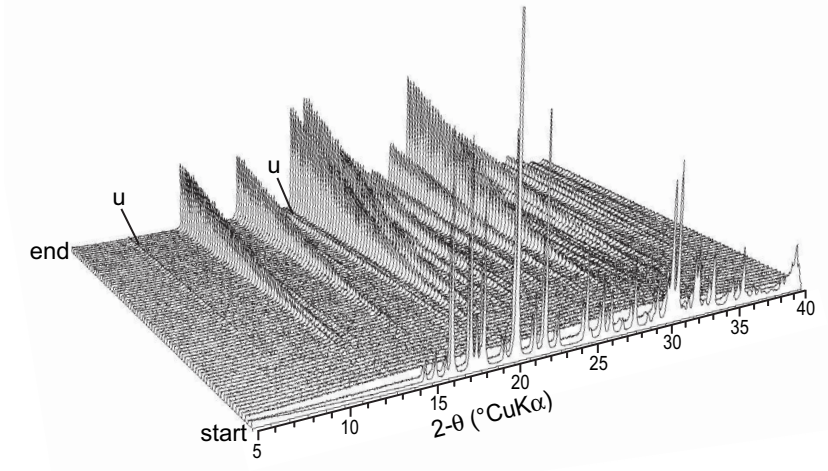

FIGURE 5. Environmental cell data; 72 XRD scans collected at 336 K with RH in the cell controlled at 6%. The starting material (front of the figure) is hexahydrite before ramping temperature to 336 K. Each diffraction pattern represents a 4 h diffraction scan from 2 to 70 °2θ (Cu$K\alpha$; for clarity only the range from 5 to 40 °2θ is shown). Within 8 h, all of the hexahydrite diffraction peaks have disappeared, indicating that the sample became amorphous. It remained amorphous for ~48 h before diffraction peaks for sanderite and lesser amounts of a second, unidentified phase (peaks labeled "u") began to appear.

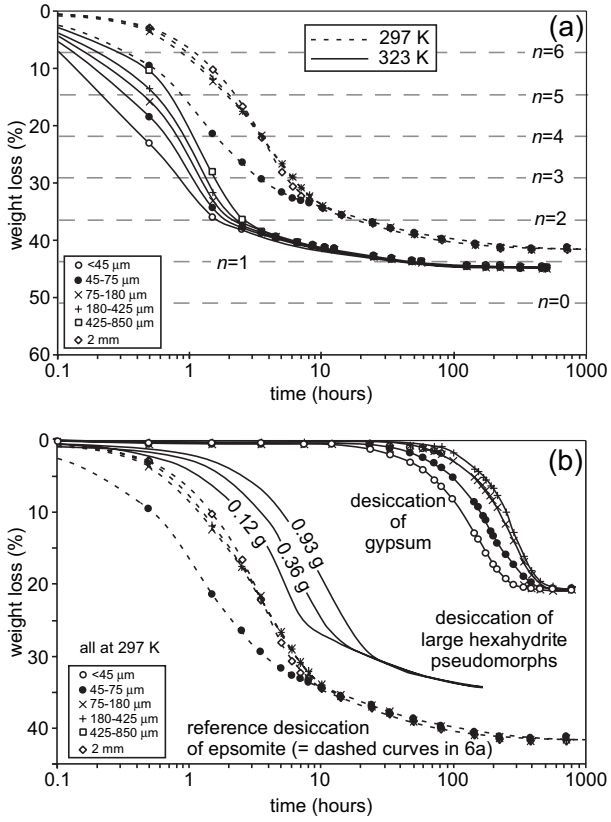

FIGURE 6. Long-term dehydration of Mg- and Ca-sulfate salts at P_{H_2O} ~0.7 Pa. Upper panel (**a**) shows results for several size fractions of epsomite at two temperatures; dashed horizontal lines indicate the values of *n* along the weight loss curves shown. Lower panel (**b**) compares results for gypsum size fractions, large hexahydrite crystals (solid curves without symbols; the middle curve correlates with the transition between Figs. 1b and 1c), and the epsomite size fractions at 297 K and P_{H_2O} of ~0.7 Pa (dashed curves) from panel **a**.

vacuum conditions for longer than shown in Figure 6; from 4000 to 6000 h the residual water content remained unchanged. The residual water content after long vacuum desiccation increases with decrease in the temperature at which desiccation occurs for a given P_{H_2O}. Further experimental data are being collected at lower temperatures to develop a full model of *n*-temperature-time-P_{H_2O} for the amorphous phase, and to constrain the low-temperature conditions where crystalline rather than amorphous forms may persist even at vacuum.

In another experiment, size fractions of natural gypsum from Bingham, New Mexico, were held at the 297 K conditions in the vacuum chamber. In Figure 6b, the weight loss curves for the gypsum size fractions are compared with the loss curves for two $MgSO_4 \cdot nH_2O$ samples held at the same conditions: the 297 K set of epsomite curves from Figure 6a and weight loss curves for three large hexahydrite pseudomorphs after epsomite of 0.12 g to 0.93 g (solid curves without symbols; the middle curve follows dehydration of the hexahydrite pseudomorph in Fig. 1b to the desiccated pseudomorph in Fig. 1c). Even though the hexahydrite pseudomorphs are considerably larger than the small grains of epsomite, at these conditions they still reach a common desiccation path within 30 h and follow a subsequent desiccation path parallel to the finer epsomite size fractions (epsomite and hexahydrite curves in Fig. 6b reach different final percentages of weight loss because the hexahydrite starts with 1/7 less water). The development of pervasive desiccation fractures within large amorphous pseudomorphs (Fig. 1c) provides an effective grain size equivalent to submillimeter size fractions.

Gypsum desiccation, even at particle sizes of <45 µm, is far more sluggish than desiccation of equivalent epsomite or hexahydrite grains. This is not unexpected given the greater thermal stability of gypsum relative to epsomite (Fig. 4), but the resistance to desiccation in vacuum is exceptional, with a delay in response that is two orders of magnitude greater than the quite rapid initiation of desiccation in epsomite or hexahydrite. As shown in Figure 6b, at 297 K and ~0.7 Pa P_{H_2O} the gypsum samples have no significant weight loss for the first 10 h of exposure; desiccation is essentially complete by 550 h, at which point the sample retains only 0.8 wt% H_2O. This residual water content is significantly less than that of the ideal hemihydrate, bassanite (6 wt% H_2O), but XRD analysis of a sample split exposed along with these size fractions shows that the desiccated residue retains the crystal structure of bassanite, even though the value of *n* is 0.06, well below the ideal value of 0.5.

Rehydration

Rehydration data at 100% RH and various temperatures were collected for samples of Mg- and Ca-sulfates with low values of *n*. Representative results are summarized in Figure 7. The upper panel (Fig. 7a), representing hydration at 100% RH over water ice at 271 K, shows hydration curves for the large amorphous pseudomorphs that were desiccated from hexahydrite pseudomorphs along the curves shown in Figure 6b. Starting weights of the amorphous pseudomorphs are shown for each curve. Figure 7a also shows hydration curves for the four size fractions of desiccated gypsum from Figure 6b.

Figure 7b compares long-term rehydration of unsieved amorphous $MgSO_4 \cdot nH_2O$ samples (≤425 µm) with $n = 1.2$ at 100% RH at four temperatures (dashed curves), as well as hydration of kieserite at the two coldest temperatures (solid curves). The amorphous $MgSO_4 \cdot nH_2O$ was synthesized by exposure of unsieved hexahydrite powder at a P_{H_2O} of ~0.7 Pa and 297 K for 4000 h. A finer (~5 µm) kieserite powder was synthesized by placing anhydrous $MgSO_4$ over a saturated $SrCl_2$ salt solution at 348 K for more than 3 weeks. For the amorphous phase, hydration weight gain of 72% results from the acquisition of sufficient water to form epsomite. For kieserite, the weight gain required to form epsomite is 76%. Both of these values are within the thickness of the dashed horizontal line representing rehydration to epsomite at the top of Figure 7b (paths going above this line represent deliquescence). Exposures to 100% RH over water at $T > 273$ K, attempted only with the amorphous sample, resulted in rapid hydration and only a brief delay at the epsomite line before the samples began to deliquesce. For both the amorphous sample and kieserite, rehydration over water ice at $T < 273$ K resulted in formation of epsomite without deliquescence, at rates dependent on both temperature and nature of the starting phase. All of the amorphous starting materials remain powders as they expand on rehydration, but we have noted in ongoing studies that kieserite

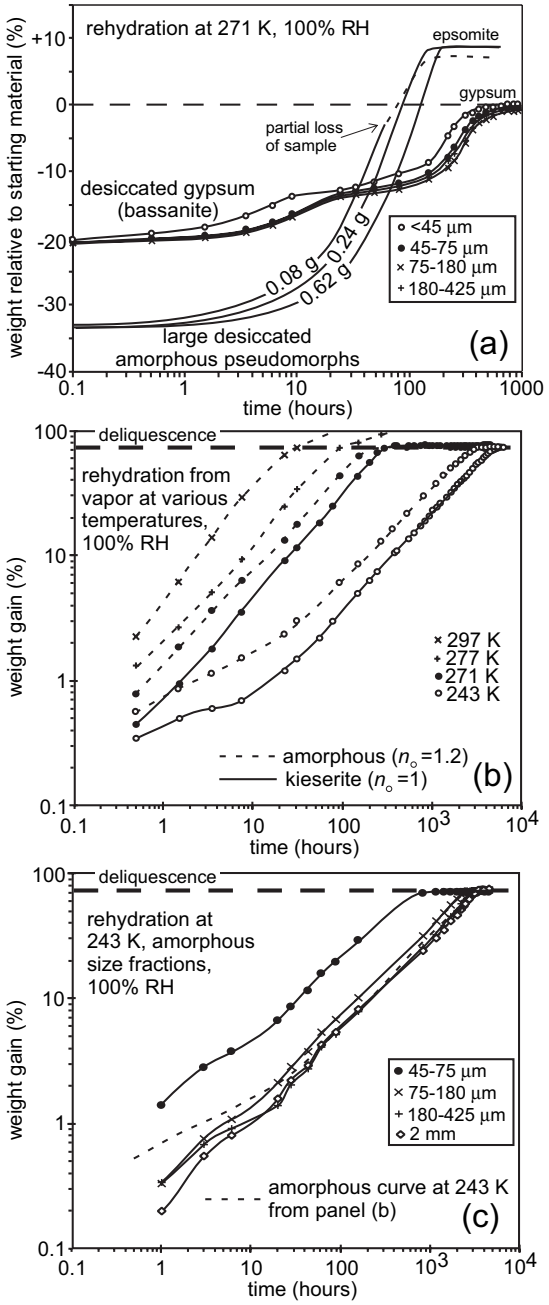

FIGURE 7. Rehydration curves at 100% RH for (**a**) size fractions of desiccated gypsum (bassanite) grains and amorphous pseudomorphs of large, desiccated epsomite crystals at 271 K, (**b**) amorphous $MgSO_4{\cdot}nH_2O$ (short-dashed curves) and kieserite (solid curves) at four different temperatures, and (**c**) size fractions of amorphous $MgSO_4{\cdot}nH_2O$ at 243 K (solid curves) along with the unsieved 243 K sample (short-dashed curve) from panel **b**. Long-dashed horizontal lines in **b** and **c** represent complete rehydration to epsomite. Note that the vertical axis in **a** shows weight relative to the gypsum or hexahydrite starting material in Figure 6b (solid curves in that figure); rehydrated gypsum returns to zero difference from the initial gypsum, but formation of epsomite results in 8% weight gain relative to the initial hexahydrite. The middle solid curve of the three desiccated amorphous pseudomorphs in **a**, labeled with the amorphous pseudomorph starting weight of 0.24 g, correlates with the transition between Figures 1c and 1d.

powders rehydrated at 243 K grow together to form a cemented crust (Vaniman et al. 2006). Nevertheless, the slope of the 243 K rehydration curve for kieserite in Figure 7b is parallel to that for the amorphous powder at the same temperature, suggesting that the cemented kieserite mass remains porous enough that hydration rate is not reduced.

Figure 7c examines grain-size effects in rehydration rates of amorphous $MgSO_4{\cdot}nH_2O$ at a single temperature, 243 K. Sieved fractions of epsomite were first desiccated at 293 K and 0.7 Pa P_{H_2O} to create amorphous $MgSO_4{\cdot}nH_2O$ of n = 1.2; these size fractions were then rehydrated at 100% RH relative to water ice as shown in Figure 7c. The unsieved fraction from Figure 7b that was rehydrated at the same conditions is included for comparison. There is little grain-size effect for particles >75 µm, but at 45–75 µm, the hydration rate at these conditions is greater by a factor of ~4, reaching epsomite formation within ~700 vs. ~3000 h.

The results shown in Figure 7a indicate that the large anhydrous pseudomorphs rehydrated at 271 K and 100% RH convert to epsomite within ~100 h. This transition is relatively continuous, with no obvious inflections in the hydration curves. In contrast, the desiccated bassanite rehydrates in two stages, first acquiring water to a content ~40% above that of ideal bassanite within ~10 h, and then following a second-stage hydration to gypsum in ~650 h. Rehydration in the $CaSO_4{\cdot}nH_2O$ system is more complex than in $MgSO_4{\cdot}nH_2O$. This complexity is not unexpected considering the problems pursued in the extensive literature on the industrially important $CaSO_4{\cdot}nH_2O$ system (e.g., Hand 1994). Work is in progress to obtain a more complete understanding of the $CaSO_4$ system at the very low P_{H_2O} conditions representative of Mars.

The results in Figure 7b provide reaction rates at four temperatures for samples of amorphous $MgSO_4{\cdot}nH_2O$. Disregarding the weight data for deliquescence above 273 K, these curves can be used to obtain an understanding of the timespans required for desiccated, amorphous $MgSO_4{\cdot}nH_2O$ to form epsomite at lower latitudes on Mars when diurnal, seasonal, or obliquity cold periods favor condensation of water frost or ice. Although further data are needed to derive a similar understanding for kieserite, the data shown for 271 and 243 K, compared with those for the amorphous form at these temperatures, indicate that the timespans required for equivalent kieserite hydration are approximately twice those for the amorphous phase, even though the kieserite sample in Figure 7b is finer-grained.

For the lowest-temperature rehydration pathways in Figure 7b, consumable splits of both amorphous and kieserite forms were run along with the samples that were used for weight tracking. Analysis of these splits by XRD shows that the amorphous form begins to recrystallize to hexahydrite that increases in abundance and persists until sufficient water is acquired to attain n = 7, at which point the superhydrated hexahydrite recrystallizes to epsomite. In contrast, the kieserite forms small amounts of hexahydrite at first, but epsomite appears early in the hydration sequence, well below a hydration value of n = 7, and gradually displaces both hexahydrite and kieserite (Vaniman et al. 2006).

Variable rates due to grain size, illustrated in Figure 7c, show that for amorphous $MgSO_4{\cdot}nH_2O$, the particle size has little

effect above 75 μm. However, hydration rates are significantly faster for finer particles (silt size and finer). In this size range, particles are subject to suspension by winds on Mars (Edgett and Christensen 1994); the most reactive of the $MgSO_4 \cdot nH_2O$ particles in the soil are thus also those most susceptible to planet-wide distribution.

Hydration cycling

Cycling of temperature and water vapor pressure at the martian surface occurs on daily and seasonal cycles, as well as over longer timespans where obliquity can have the effect of redistributing polar ice to lower latitudes. The most severe temperature swings at the martian surface occur at the equator, where summer daytime temperatures of exposed soil can reach 290 K and, at night, the soil surface temperature drops to 180–190 K (Smith et al. 2004). This short and severe cycle exposes hydrous phases to rapidly changing conditions of <1% RH by early afternoon and 100% RH in the early morning hours (Savijarvi 1995; Zent et al. 2001).

In Figure 8, we summarize the results of a simple experiment to determine the likely fate of epsomite grains either carried to the equator by dust storms or excavated from a sedimentary deposit at a depth where porespace P_{H_2O} favors epsomite stability. This experiment exceeds the extremes of a summer day by desiccating the samples at 297 K and 0.7 Pa P_{H_2O} for a full 8 h in each cycle, which favors desiccation, but it also allows a greatly accelerated rate of nighttime hydration by exposing the sample for 12 h in each cycle to 100% RH at 243 K rather than 190 K. The result is rapid initial weight loss with formation of an amorphous hydrate that is capable of partial rehydration at nighttime conditions, but is depleted again during the day. Repeated cycles at these conditions suggest convergence toward a value of *n* between 1 and 2. Note that the finer particles (<45 μm) rehydrate more than the coarser particles at nighttime conditions. The actual final value of *n* will depend on season, latitude, and orbital parameters, particularly where atmospheric P_{H_2O} is enhanced at high obliquity (Mischna et al. 2003). Although this experiment is simplified, it is sufficient to illustrate the likely amorphous and relatively desiccated fate of epsomite or hexahydrite exposed at the martian equatorial surface under present martian conditions.

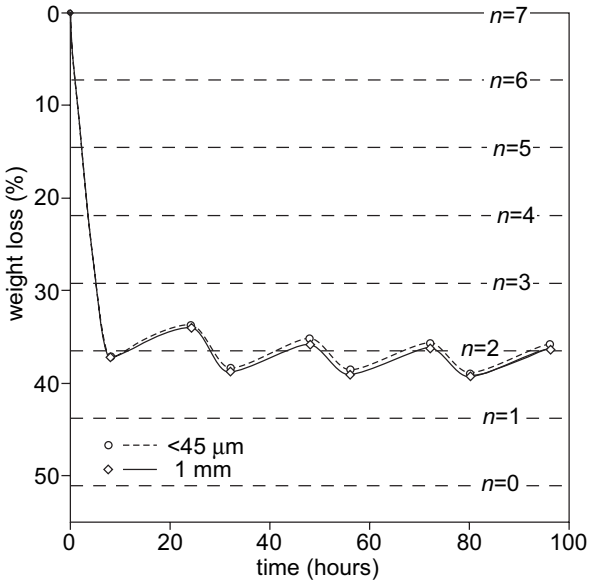

FIGURE 8. Hydration cycling in two size fractions of epsomite exposed to four 24 h cycles of alternating conditions of 8 h at 297 K and ~0.7 Pa P_{H_2O} (~0.02% RH) and 16 h at 243 K and 100% RH. Full recovery to epsomite is not possible at these conditions and the partially rehydrated forms remain amorphous, although small amounts of hexahydrite may begin to form in each hydration cycle (Vaniman et al. 2006).

DISCUSSION

Figure 9a is a plot of temperature vs. relative humidity, contoured for P_{H_2O}, with the epsomite-hexahydrite-solution stability boundaries of Chou and Seal (2003) superimposed. Also shown, as a shaded pattern, is a temperature-RH diurnal cycle for the martian equator (Pathfinder site) in late summer (Savijarvi 1995). The excursion into daytime warmer and drier conditions at the surface of an equatorial soil will expose a hydrated Mg-sulfate such as epsomite or hexahydrite to thermal conditions that speed reaction, and the reaction will be toward a desiccated, amorphous, but still partially hydrated state. The state of hydration will be higher at lower temperature (Fig. 6a); thus, the amount of water held by the amorphous form will be greater where daytime temperatures are lower. There is likely to be a continuum of water contents in the amorphous form, from *n* values no lower than ~1 at the warmest possible equatorial surface to values possibly as high as 7 as latitude increases. Thus, the amorphous form in most surface soils is likely to hold more water than kieserite. As noted above, the more robust structure of kieserite is likely to survive indefinitely under dry equatorial conditions. Gypsum, with intermediate resistance to dehydration (Figs. 4 and 6b), may also survive under these conditions, but existing data are not yet conclusive.

The dashed curves in Figure 7b allow estimation of the timespans of exposure to conditions of 100% RH (frost or ice condensation at the surface) that would be required to transform the amorphous form with 15 wt% H_2O (n = 1.2) to epsomite with 51 wt% H_2O (this estimation applies to all particles coarser than silt; finer particles will hydrate more rapidly as shown in Fig. 7c). Figure 9b uses the curves for hydration of amorphous $MgSO_4 \cdot 1.2H_2O$ in Figure 7b to develop a four-point curve of time vs. temperature, against which the time available at 100% RH for a martian night, a winter, and an episode of high obliquity can be compared. Although the extension of the curve in Figure 9b to temperatures lower than 243 K is poorly constrained, the data are sufficient to indicate that it would require an episode of high obliquity with long-term redistribution of polar ice to the equator to convert desiccated, amorphous $MgSO_4 \cdot 1.2H_2O$ into epsomite at low latitudes.

One of the goals of this study was to evaluate the role that particular sulfate salt hydrates play in holding near-surface water near the martian equator. The situation represented in Figure 9b is an extreme representation of the case for desiccated salt. First, this image of strongly desiccated $MgSO_4 \cdot nH_2O$ salt at the surface only applies to latitudes lower than ~60–70°; at higher latitude, near-surface ice is stable and the cold but persistent situation of high soil RH will favor epsomite stabilization. Second, the actual value of *n* in the desiccated form of $MgSO_4 \cdot nH_2O$ is likely to be

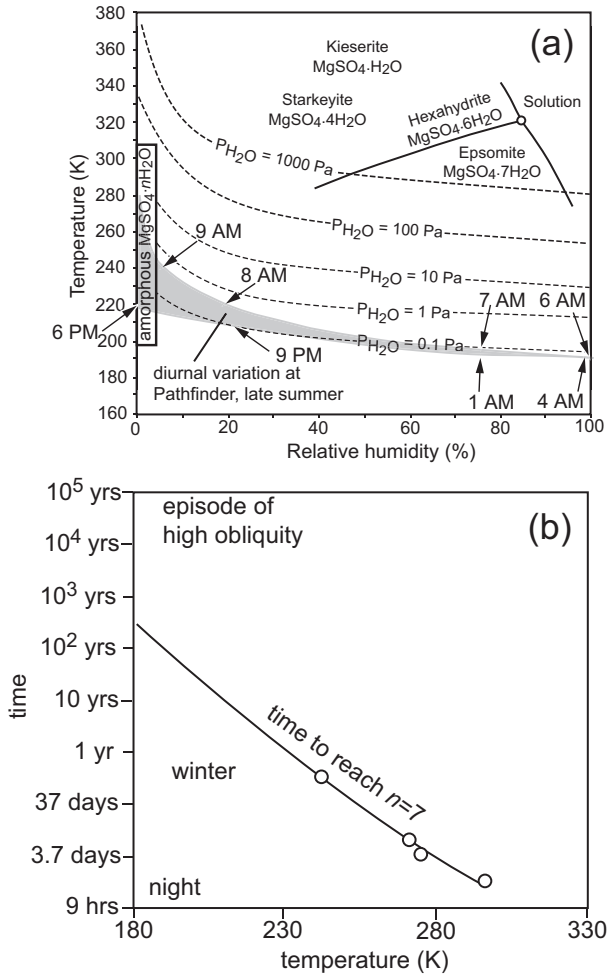

FIGURE 9. Upper panel (**a**) shows stability fields for $MgSO_4 \cdot nH_2O$ relative to temperature and RH, contoured for P_{H_2O}. Solid curves show the epsomite-hexahydrite-solution boundaries determined by Chou and Seal (2003). Fields for kieserite and starkeyite refer to preliminary results from Chipera and Vaniman (submitted); shaded region represents diurnal temperature-RH cycling in late summer at the equator (Savijarvi 1995). The field labeled "amorphous $MgSO_4 \cdot nH_2O$" represents the region where we have shown that epsomite and hexahydrite will desiccate to metastable amorphous forms; warmest and most reactive portion of the day-night cycle is within this field. Panel (**b**) uses the dashed hydration curves in Figure 7b to predict the time required at a given temperature and 100% RH (water or water-ice vapor present) to fully rehydrate an amorphous precursor to epsomite ($n = 7$). Time-temperature conditions at high RH for equatorial night and for winter fall below the curve and will not have sufficient time for complete rehydration to epsomite; equatorial redistribution of ice in an episode of high obliquity may provide sufficient time, although more data at low temperature are required to better define cold-condition rehydration rates.

greater than 1.2, considering that effective desiccation is likely to have taken place at an average daytime temperature lower than the 297 K used in our coldest desiccation experiment and residual water content rises at lower temperatures (Fig. 6a). Finally, this scenario only applies to the uppermost surface of regolith at the equator under present conditions. The diurnal variation in temperature and RH will dampen at the regolith skin depth for these parameters, which will vary with factors such as thermal inertia, albedo, diffusivity, and slope exposure of the regolith, but will in most cases be several centimeters to a few decimeters (Möhlmann 2004; Schorghofer et al. 2002; Schorghofer and Aharonson 2005). Below the skin depth, averaged conditions of ~220 K with moderated RH may preserve epsomite indefinitely at depth within the regolith. This has particular significance for orbital measurements that use neutrons to probe for water, because the effective depth of this method is ~1 m (Feldman et al. 2004a), which in most soils will be greater than the skin depth. Although $MgSO_4 \cdot nH_2O$ may be desiccated to a content of only ~15 wt% H_2O at the very surface, at greater depths but within the neutron signal volume there may be significant amounts of epsomite with 51 wt% H_2O. Estimates of typical $MgSO_4$ content in soils range to ~10 wt% on an anhydrous basis, most concentrated in shallow, cemented soil (Toulmin et al. 1977; Larsen et al. 2000). Water associated with such an $MgSO_4$ abundance, if present as epsomite, could account for most of the 10% H_2O-equivalent hydrogen observed by the Odyssey neutron spectrometer in some equatorial regions (Feldman et al. 2004a).

One of the implications of this study is the vulnerability of kieserite on Mars. Work in progress (Chipera et al. 2005; Chipera and Vaniman 2006) indicates that in the vapor-solid system, kieserite requires temperatures considerably warmer than martian equatorial summer for stable synthesis (Fig. 9a). Once it has been formed, kieserite requires more energy to desiccate than other forms of $MgSO_4 \cdot nH_2O$ (Fig. 4). Although kieserite resists desiccation at low RH, it cannot resist hydration to epsomite with prolonged exposure to high RH (Fig. 7b). Kieserite on Mars, once brought to the surface, is likely to be exposed eventually at either a high-latitude zone of persistent 100% RH conditions or an equatorial zone where periodic episodes of high obliquity and equatorial ice stabilization will bring it into conditions where it will hydrate to epsomite (Fig. 9b). Once converted to epsomite, on desiccation at surface temperature-RH conditions, it cannot revert to kieserite but can become amorphous. Enclaves of persistent low RH would be required to preserve kieserite, and confirmation of crystalline kieserite in martian equatorial regolith would provide evidence that prolonged ice distribution across the planet during past epochs has not been universal. Perhaps such enclaves have been discovered in near-equatorial regions by the OMEGA spectrometer on Mars Express, particularly in layered deposits within and near Valles Marineris (Bibring et al. 2005; Gendrin et al. 2005), although further work is needed to determine if kieserite can be distinguished clearly in visible-IR spectroscopy from amorphous Mg-sulfate having similarly low water content.

The ease with which Mg-sulfate brines react with some Ca-bearing silicate phases to form gypsum (Figs. 2 and 3) points to likely assemblages containing both $MgSO_4 \cdot nH_2O$ and $CaSO_4 \cdot nH_2O$. This observation is in line with indications that the sulfate salt constituents in sediments at Meridiani Planum include both Mg- and Ca-sulfates (Squyres et al. 2004). Both sulfates have been catalogued as secondary phases in martian meteorites, although the case for an origin on Mars is stronger for $CaSO_4 \cdot nH_2O$ than for $MgSO_4 \cdot nH_2O$ (Gooding et al. 1991). Both sulfates have also been formed in acid-fog weathering experi-

ments using basalts (e.g., Tosca et al. 2004). These occurrences, along with the data presented here for reactive coprecipitation, suggest that the $MgSO_4{\cdot}nH_2O$ - $CaSO_4{\cdot}nH_2O$ association may be widespread on Mars, in sediments and in soils that derive their salts from erosion of sediments, from acid weathering of rocks, or from periodic brine-regolith interactions that persist to the present (Knauth and Burt 2002). Aeolian distribution can spread these salts globally; in fine-grained silt subject to widest distribution both desiccation and hydration rates will be enhanced. Where these fine particles accumulate, humidity cycling and the action of thin films of adsorbed water that will behave as if liquid (Möhlmann 2004) may produce, over long timespans, the slightly indurated salt "duricrust" that is widespread at cm-scale depths in martian regolith.

Figure 10 is a sketch of martian equatorial regolith progressing from a past episode of high obliquity to present dry conditions. The diagram at the top (Fig. 10a) indicates a thin and irregular accumulation of water ice, partially covering both regolith and outcrops. Persistence of equatorial ice for high-obliquity timescales of ~10^4–10^5 years will favor full hydration of any precursor form of $MgSO_4{\cdot}nH_2O$, amorphous or crystalline, to form epsomite. A duricrust, enriched in $MgSO_4{\cdot}nH_2O$, has swollen through hydration from low values of n to $n = 7$ (epsomite); at about 10% $MgSO_4$ in this crust (water-free weight basis), a volume expansion of approximately 7% will result. If swelling clays are present, they will contribute to further expansion.

The lower diagram (Fig. 10b) shows the same equatorial soil profile, but at present conditions with obliquity at a relatively small value. All near-equatorial regolith ice is gone, and variable desiccation has occurred within the skin depths of diurnal and seasonal fluctuation (centimeters to several decimeters, depending on local thermal inertia, albedo, diffusivity, and slope: Möhlmann 2004; Schorghofer et al. 2002; Schorghofer and Aharonson 2005). Noonday and early afternoon heating of the upper regolith, and heat dissipated from dark basaltic boulders into surrounding soil, favor the desiccation of epsomite in the upper few centimeters, possibly into and through the duricrust, resulting in desiccation cracks in the duricrust as observed at the Viking 1

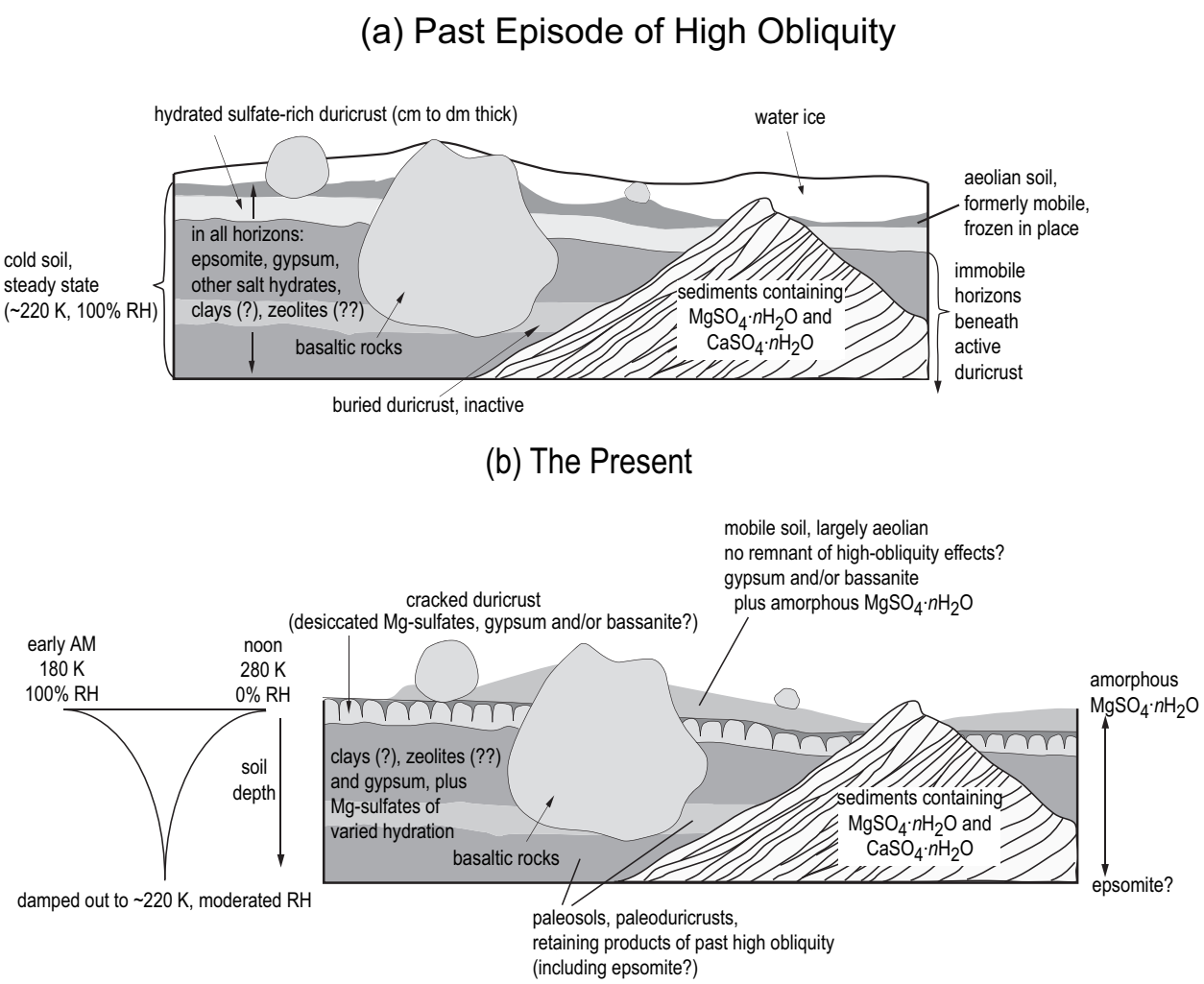

FIGURE 10. Schematic representation of equatorial martian regolith under water ice during a past episode of high obliquity (**a**), contrasted with current conditions (**b**). Panel **b** is modified after Retallack (1990), based on Sharp and Malin (1984).

site. Surficial clays, but less likely zeolites, may "breathe" on a diurnal cycle (Bish et al. 2003; Tokano and Bish 2005). The fate of $CaSO_4 \cdot nH_2O$ in this system is less certain, but initial evidence suggests that it may resist desiccation (Fig. 6b). Below the skin depth, conditions are dampened out to a cold average temperature and moderated RH at which epsomite and gypsum both may be stable, and clays or zeolites will be at relatively full hydration. The inventory of hydrous minerals below the skin depth may contain ancient water, augmented only sparingly by downward vapor diffusion when ice is at the surface during high obliquity (Schorghofer and Aharonson 2005) and relatively immune from extraction during low obliquity.

Exposed at the surface is the active aeolian system that periodically exposes the duricrust, ensuring that many portions of this salt-cemented horizon are likely to experience the full impact of thermal and RH cycling during some episodes of low obliquity, even if they are blanketed by dust, silt, and sand at other times. Highly desiccated salt hydrates and hydrous silicates in the silt size range are mobile and may be rehydrated by transport to higher latitudes, or desiccated if transported from higher latitudes to the equator. Depending on latitude, this activity may occur on timescales close enough to the epsomite-formation threshold (Fig. 9b) that in situ determination of dust and soil hydration states might be used to date soils and define regolith dynamics on Mars.

ACKNOWLEDGMENTS

This work was performed under the auspices of the U.S. Department of Energy (DOE) under contract W-7405-ENG-36 with the University of California. The research project was supported by Los Alamos National Laboratory Directed Research and Development funding. Reviews by B. Jolliff and H. Newsom and editorial handling by C. Shearer contributed much to the improvement of this paper. The first author is indebted to J. J. Papike, who first introduced him to the wealth of information deposited in planetary regoliths.

REFERENCES CITED

Adam, C.D. (2003) Atomistic modeling of the hydration of $CaSO_4$. Journal of Solid State Chemistry, 174, 141–151.

Allen, C.C., Morris, R.V., Jager, K.M., Golden, D.C., Lindstrom, D.J., Lindstrom, M.M., and Lockwood, J.P. (1998) martian regolith stimulant JSC Mars-1. Lunar and Planetary Science, XXIX, Abstract no. 1690, Lunar and Planetary Institute, Houston (CD-ROM).

Ames, L.L., Jr. (1961) Cation sieve properties of the open zeolites chabazite, mordenite, erionite, and clinoptilolite. American Mineralogist, 46, 1120–1131.

Aref, M.A.M. (2003) Classification and depositional environments of Quaternary pedogenic gypsum crusts (gypcrete) from east of the Fayum Depression, Egypt. Sedimentary Geology, 155, 87–108.

Baird, A.K., Toulmin, P., III, Clark, B.C., Rose, H.J., Jr., Keil, K., Christian, R.P., and Gooding, J.L. (1976) Mineralogic and petrologic implications of Viking geochemical results from Mars: Interim report. Science, 194, 1288–1293.

Banin, A., Han, F.X., and Cicelsky, A. (1997) Acidic volatiles and the Mars soil. Journal of Geophysical Research, 102, 13341–13356.

Basilevsky, A.T., Litvak, M.L., Mitrofanov, I.G., Boynton, W.V., Saunders, R.S., and Head, J.W. (2003) Search for traces of chemically bound water in the martian surface layer based on HEND measurements onboard the 2001 Mars Odyssey spacecraft. Solar System Research, 37, 387–396.

Bibring, J.-P., Langevin, Y., Gendrin, A., Gondet, B., Poulet, F., Berthé, M., Soufflot, A., Arvidson, R., Mangold, N., Mustard, J., Drossart, P., and the OMEGA team (2005) Mars surface diversity as revealed by the OMEGA/Mars Express observations. Science, 307, 1576–1581.

Bish, D.L., Carey, J.W., Vaniman, D.T., and Chipera, S.J. (2003) Stability of hydrous minerals on the martian surface. Icarus, 164, 96–103.

Bonello, G., Berthet, P., and d'Hendecourt, L. (2005) Identification of magnesium sulfate hydration state derived from NIR reflectance spectroscopy. Lunar and Planetary Science, XXXVI, Abstract no. 1996, Lunar and Planetary Institute, Houston (CD-ROM).

Bridges, J.C., Catling, D.C., Saxton, J.M., Swindle, T.D., Lyon, I.C., and Grady, M.M. (2001) Alteration assemblages in martian meteorites: Implications for near-surface processes. Space Science Reviews, 96, 365–392.

Chipera, S.J. and Vaniman, D.T. (2006) Experimental stability of magnesium sulfate hydrates that may be present on Mars. Geochimica et Cosmochimica Acta, in press.

Chipera, S.J., Carey, J.W., and Bish, D.L. (1997) Controlled-humidity XRD analyses: Application to the study of smectite expansion/contraction. In J.V. Gilfrich, I.C. Noyan, R. Jenkins, T.C. Huang, R.L. Snyder, D.K. Smith, M.A. Zaitz, and P.K. Predecki, Eds., Advances in X-ray Analysis, 39, p. 713–722. Plenum, New York.

Chipera, S.J., Vaniman, D.T., Bish, D.L., Carey, J.W., and Feldman, W.C. (2005) Experimental stability and transformation kinetics of magnesium sulfate hydrates that may be present on Mars. Lunar and Planetary Science, XXXVI, Abstract no. 1497, Lunar and Planetary Institute, Houston (CD-ROM).

Chou, I.-M. and Seal, R.R., II (2003), Determination of epsomite-hexahydrite equilibria by the humidity-buffer technique at 0.1 MPa with implications for phase equilibria in the system $MgSO_4$-H_2O. Astrobiology, 3, 619–630.

Clark, B.C. (1978) Implications of abundant hygroscopic minerals in the martian regolith. Icarus, 34, 645–665.

——— (1993) Geochemical components in martian soil. Geochimica et Cosmochimica Acta, 57, 4575–4581.

Clark, B.C. and Van Hart, D.C. (1981) The salts of Mars. Icarus, 45, 370–378.

Clark, B.C., Morris, R.V., McLennan, S.M., Gellert, R., Jolliff, B., Knoll, A.H., Squyres, S.W., Lowenstein, T.K., Ming, D.W., Tosca, N.J., and others (2005) Chemistry and mineralogy of outcrops at Meridiani Planum. Earth and Planetary Science Letters, 240, 73–94.

Edgett, K.S. and Christensen, P.R. (1994) Mars Aeolian sand: Regional variations among dark-hued crater floor features. Journal of Geophysical Research, 99, 1997–2018.

Feldman, W.C., Prettyman, T.H., Maurice, S., Plaut, J.J., Bish, D.L., Vaniman, D.T., Mellon, M.T., Metzger, A.E., Squyres, S.W., Karunatillake, S., and others (2004a) Global distribution of near-surface hydrogen on Mars. Journal of Geophysical Research, 101, E09006, DOI: 10.1029/2003JE002160.

Feldman, W.C., Mellon, M.T., Maurice, S., Prettyman, T.H., Carey, J.W., Vaniman, D.T., Bish, D.L., Fialips, C.I., Chipera, S.J., Kargel, J.S., and others (2004b) Hydrated states of $MgSO_4$ at equatorial latitudes on Mars. Geophysical Research Letters, 31, L16702, DOI: 10.1029/2004GL020181.

Fialips, C.I., Carey, J.W., and Bish, D.L. (2005a) Hydration-dehydration behavior and thermodynamics of chabazite. Geochimica et Cosmochimica Acta, 69, 2293–2308.

Fialips, C.I., Carey, J.W., Vaniman, D.T., Bish, D.L., Feldman, W.C., and Mellon, M.T. (2005b) Hydration state of zeolites, clays, and hydrated salts under present-day martian surface conditions: Can hydrous minerals account for Mars Odyssey observations of near-equatorial water-equivalent hydrogen? Icarus, 178, 74–83.

Follner, S., Wolter, A., Preusser, A., Indris, S., Silber, C., and Follner, H. (2002) The setting behaviour of α- and β-$CaSO_4 \cdot 0.5H_2O$ as a function of crystal structure and morphology. Crystal Research and Technology, 37, 1075–1087.

Gendrin, A., Mangold, N., Bibring, J.-P., Langevin, Y., Gondet, B., Poulet, F., Bonello, G., Quantin, C., Mustard, J., Arvidson, R., and LeMouélic, S. (2005) Sulfates in martian layered terrains: The OMEGA/Mars Express view. Science, 307, 1587–1591.

Gooding, J.L., Wentworth, S.J., and Zolensky, M.E. (1991) Aqueous alteration of the Nakhla meteorite. Meteoritics, 26, 135–143.

Grodzicki, A. and Piszczek, P. (1998) A new interpretation of abnormal shift of water molecules' bending vibration frequencies in kieserite family monohydrates. Journal of Molecular Structure, 443, 141–147.

Hand, R.J. (1994) The kinetics of hydration of calcium sulphate hemihydrate: A critical comparison of the models in the literature. Cement and Concrete Research, 24, 885–895.

Hawthorne, F.C., Krivovichev, S.V., and Burns, P.C. (2000), The Crystal Chemistry of Sulfate Minerals. In C.N. Alpers, J.L. Jambor, and D.K. Nordstrom, Eds., Sulfate Minerals: Crystallography, Geochemistry, and Environmental Significance, 40, p. 1–112. Reviews in Mineralogy and Geochemistry, Mineralogical Society of America, Chantilly, Virginia.

Head, J.W., Mustard, J.F., Kreslavsky, M.A., Milliken, R.E., and Marchant, D.R. (2003) Recent ice ages on Mars. Nature, 426, 797–802.

Klingelhöfer, G., Morris, R.V., Bernhardt, B., Schröder, C., Rodionov, D.S., de Souza, P.A., Jr., Yen, A., Gellert, R., Evlanov, E.N., Zubkov, B., and others (2004) Jarosite and hematite at Meridiani Planim from Opportunity's Mössbauer spectrometer. Science, 306, 1740–1745.

Knauth, L.P. and Burt, D.M. (2002) Eutectic brines on Mars: Origin and possible relation to young seepage features. Icarus, 158, 267–271.

Lane, M.D. (2005) Evidence for aqueously precipitated sulfates in northeast Meridiani using THEMIS and TES data. Lunar and Planetary Science, XXXVI, Abstract no. 2180, Lunar and Planetary Institute, Houston (CD-ROM).

Lane, M.D., Dyar, M.D., and Bishop, J.L. (2004) Spectroscopic evidence for hydrous iron sulfate in the martian soil. Geophysical Research Letters, 31, L19702, DOI: 10.1029/2004GL021231.

Langevin, Y., Poulet, F., Bibring, J.-P., and Gondet, B. (2005) Sulfates in the north polar region of Mars detected by OMEGA/Mars Express. Science, 307, 1584–1586.

Larsen, K.W., Arvidson, R.E., Jolliff, B.L., and Clark, B.C. (2000) Correspondence and least-squares analyses of soil and rock compositions for the Viking Lander 1 and Pathfinder landing sites. Journal of Geophysical Research, 105, 29207–29221.

Mellon, M.T. and Jakosky, B.M. (1993) Geographic variations in the thermal and diffusive stability of ground ice on Mars. Journal of Geophysical Research, 98, 3345–3364.

——— (1995) The distribution and behavior of martian ground ice during past and present epochs. Journal of Geophysical Research, 100, 11781–11799.

Mischna, M.A., Richardson, M.I., Wilson, R.J., and McCleese, D.J. (2003) On the orbital forcing of martian water and CO_2 cycles: A general circulation model study with simplified volatile schemes. Journal of Geophysical Research, 108, E65062, DOI: 10.1029/2003JE002051.

Möhlmann, D.T.F. (2004) Water in the upper martian surface at mid- and low-latitudes; presence, state, and consequences. Icarus, 168, 318–323.

Poulet, F., Bibring, J.-P., Mustard, J.F., Gendrin, A., Mangold, N., Langevin, Y., Arvidson, R.E., Gondet, B., Gomez, C., and the Omega Team (2005) Phyllosilicates on Mars and implications for early martian climate. Nature, 438, 623–627.

Retallack, G.J. (1990) Soils of the past, 520 p. Unwin Hyman, Winchester, Massachusetts.

Rieder, R., Gellert, R., Anderson, R.C., Brückner, J., Clark, B.C., Dreibus, G., Economou, T., Klingelhöfer, G., Lugmair, G.W., Ming, D.W., and others (2004) Chemistry of rocks and soils at Meridiani Planum from the alpha particle X-ray spectrometer. Science, 306, 1746–1749.

Ruff, S.W. (2004) Spectral evidence for zeolite in the dust on Mars. Icarus, 168, 131–143.

Savijarvi, H. (1995) Mars boundary layer modeling: Diurnal moisture cycle and soil properties at the Viking Lander 1 site. Icarus, 117, 120–127.

Schorghofer, N. and Aharonson, O. (2005) Stability and exchange of subsurface ice on Mars. Journal of Geophysical Research, 110, E05003, DOI: 10.1029/2004JE002350.

Schorghofer, N., Aharonson, O., and Khatiwala, S. (2002) Slope streaks on Mars: Correlations with surface properties and the potential role of water. Geophysical Research Letters, 29, no. 232126, DOI: 10.1029/2002GL015889.

Sharp, R.P. and Malin, M.C. (1984) Surface geology from Viking landers on Mars: A second look. Geological Society of America Bulletin, 95, 1398–1412.

Sheppard, R.A. and Gude, A.J., III (1982) Mineralogy, chemistry, gas adsorption, and NH_4^+-exchange capacity for selected zeolitic tuffs from the western United States. United States Geological Survey, Open-File Report 82-969, 16 p.

Singer, A., Kirsten, W.F.A., and Bühmann, C. (1999) A proposed fog deposition mechanism for the formation of sulfate efflorescences in the Mpumalanga highveld, Republic of South Africa. Water, Air, and Soil Polution, 109, 313–325.

Smith, M.D., Wolff, M.J., Lemmon, M.T., Spanovich, N., Banfield, D., Budney, C.J., Clancy, R.T., Ghosh, A., Landis, G.A., Smith, P., and others (2004) First atmospheric science results from the Mars Exploration Rovers Mini-TES. Science, 306, 1750–1753.

Solomon, S.C., Aharonson, O., Aurnou, J.M., Banerdt, W.B., Carr, M.H., Dombard, A.J., Frey, H.V., Golombek, M.P., Hauck, S.A., Head, J.W., and others (2005) New perspectives on ancient Mars. Science, 307, 1214–1220.

Squyres, S.W., Grotzinger, J.P., Arvidson, R.E., Bell, J.F., III, Calvin, W., Christensen, P.R., Clark, B.C., Crisp, J.A., Farrand, W.H., Herkenhoff, K.E., and others (2004) In situ evidence for an ancient aqueous environment at Meridiani Planum, Mars. Science, 306, 1709–1714.

Tokano, T. and Bish, D.L. (2005) Hydration state and abundance of zeolites on Mars and the water cycle. Journal of Geophysical Research, 110, E12S08, DOI: 10.1029/2005JE002410.

Tosca, N.J., McLennan, S.M., Lindsley, D.H., and Schoonen, M.A.A. (2004) Acid-sulfate weathering of synthetic martian basalt: The acid fog model revisited. Journal of Geophysical Research, 109, E05003, DOI: 10.1029/2003JE002218.

Toulmin, P., III, Baird, A.K., Clark, B.C., Keil, K., Rose, H.J., Jr., Christian, R.P., Evans, P.H., and Kelliher, W.C. (1977) Geochemical and mineralogical interpretation of the Viking inorganic chemical results. Journal of Geophysical Research, 82, 4625–4634.

Vaniman, D.T., Bish, D.L., Chipera, S.J., Fialips, C.I., Carey, J.W., and Feldman, W.C. (2004a) Magnesium sulphate salts and the history of water on Mars. Nature, 431, 663–665.

Vaniman, D.T., Chipera, S.J., Bish, D.L., Carey, J.W., Fialips, C.I., and Feldman, W.C. (2004b) Sulfate salts, regolith interactions, and water storage in equatorial martian regolith. Lunar and Planetary Science, XXXV, Abstract no. 1690, Lunar and Planetary Institute, Houston (CD-ROM).

Vaniman, D.T., Chipera, S.J., and Carey, J.W. (2006) Hydration experiments and physical observations at 193 and 243 K for Mg-sulfates relevant to Mars. Lunar and Planetary Science, XXXVII, Abstract no. 1442, Lunar and Planetary Institute, Houston (CD-ROM).

Wentworth, S.J., Gibson, E.K., Velbel, M.A., and McKay, D.S. (2005) Antarctic Dry Valleys and indigenous weathering in Mars meteorites: Implications for water and life on Mars. Icarus, 174, 383–395.

Zent, A.P., Howard, D.J., and Quinn, R.C. (2001) H_2O adsorption on smectites: Application to the diurnal variation of H_2O in the martian atmosphere. Journal of Geophysical Research, 106, 14667–14674.

Zolotov, M.Yu. (1989) Water-bearing minerals in the martian soil (thermodynamic prediction of stability). Lunar and Planetary Science, XX, 1257–1258.

MANUSCRIPT RECEIVED SEPTEMBER 16, 2005
MANUSCRIPT ACCEPTED APRIL 28, 2006
MANUSCRIPT HANDLED BY C. SHEARER